FUSION OF MORPHOLOGICAL AND TEXTURE FEATURES FOR HIGH RESOLUTION IMAGE CHANGE DETECTION

Chris Padwick, Principal Scientist
Fabio Pacifici, Principal Scientist
Giovanni Marchisio, Principal Scientist
Nathan Longbotham, Research Associate
DigitalGlobe
1601 Dry Creek Drive, Suite 260
Longmont CO, 80503, USA
cpadwick@digitalglobe.com

ABSTRACT

Timely and accurate detection of damage caused by natural disasters is extremely important for supporting better decision making during emergencies. For operational use, it is crucial to produce damage maps as soon as the post-event images are available. This is a key issue for civil governments who need a fast and preliminary overview of the epicentral area, quick information on the extension and distribution of damage, and an evaluation of infrastructure.

New imaging systems such as the WorldView-2 and WorldView-1 satellites, characterized by sub-meter spatial resolution, are now providing more imaging capacity on top of existing platforms, such as QuickBird or IKONOS, which have been operating for years. A large amount of information is available, and therefore the need for fully automated change detection techniques is becoming extremely urgent. Fully automated methods should be robust to residual mis-registrations, shadows, and seasonal and meteorological effects. These effects combine to reduce the attainable accuracy in the damage map. Moreover, since commercial sensors frequently relax constraints on collection geometries in order to increase collection opportunities during natural disasters, automated techniques must be robust to changing image acquisition angles.

KEYWORDS: Morphology, Texture, High resolution satellite imagery, change detection, data mining, machine learning, Digitalglobe, WorldView 1, WorldView 2

INTRODUCTION

The motivation behind developing a data-mining framework to assess changes over a multiple image set is particularly applicable to natural disaster monitoring and assessment. The reasons for this are several-fold:

- Generally speaking one may have images of the area of interest prior to an event and the imagery may comprise multiple modalities;
- After a major event like an earthquake or tsunami, the focus of commercial satellite imaging companies is rapid collection and dissemination of imagery for impact analysis, rescue operations, etc. Thus multiple images of the after event may be available with a variety of modalities. Generally the images will be available in an asynchronous fashion with delays ranging from minutes in the case of same pass collections;
- In general we cannot count on the availability of detailed digital surface models (or even digital elevation models that exceed the quality of SRTM-30) to assist in our analysis;
- Due to the focus on rapid collection of an area after an event, the collection geometries like off nadir angle are opened up to provide more collection opportunities. This creates challenges for change detection since the different viewing geometries create perspective viewpoint distortions that can't be modeled (see above point).

Thus we desire a framework that will allow us to:

- Estimate the changes between images in an automated fashion;
- Work with multiple modalities of imagery;
- Is robust against errors in digital elevation models since highly detailed elevation models may not be available. Such errors generally show up as mis-registration between images, even after a careful image to image registration process is applied;

- Does not require digital surface models to exist and thus is robust against errors caused by perspective viewpoint distortions that can't be modeled out of the data.

The focus of this paper is to evaluate the applicability of texture and morphological image operators, along with data mining techniques, to solve the change detection problem with high spatial resolution panchromatic imagery. The paper is organized as follows. First, morphological operations for image processing are presented and described mathematically. Next, co-occurrence texture measures are discussed and briefly reviewed. Next the study area and the experimental procedure are described. Finally, the classification results are presented and the conclusions are discussed.

MATHEMATICAL MORPHOLOGY

Mathematical morphology provides a collection of image filters (called operators) based on set theory. The effective results obtained in [1], [2] with panchromatic imagery using basic operators such as *opening* and *closing* have focused the attention of the scientific community on the use of morphological analysis for image classification. Morphological operators were used to classify remote sensed images at decametric and metric resolutions and have been highlighted as very promising tools for data analysis, as reported in [3], [4]. In [5], the authors used morphological operators for image segmentation. Pesaresi and Benediktsson [6] proposed building Differential Morphological Profiles (DMP) to account for differences in the values of the morphological profiles at different scales. These profiles were exploited in [3] and [6] for the segmentation of Indian Remote Sensing Satellite 1C (IRS-1C) panchromatic imagery, using the maximal derivative of the DMP. In [7], complete DMP was applied to IRS-1C and IKONOS panchromatic imagery. Specifically, the authors exploited reconstruction DMP with neural network classifiers and two linear feature extraction methods to reduce the redundancy in information. More recently, the extraction of morphological information from hyper-spectral imagery was addressed. In [8] and [9], the first principal component was used to extract the morphological images. In [10], extended opening and closing operators by reconstruction were investigated for target detection on both Airborne Visible/Infrared Imaging Spectrometer (AVIRIS) and Reflective Optics System Imaging Spectrometer (ROSIS) data. In [11], multi-channel and directional morphological filters were used for hyper-spectral image classification, showing its ability to account simultaneously for the scale and orientation of objects.

Morphological Operators

Morphological operators are a collection of filters based on set theory. These operators are applied to two ensembles, the image g to analyze and a structuring element B, which is a set with known size and shape that is applied to the image as a filter. When centered on a pixel x, **B** is a vector that takes into account all the values x_b of the pixels of g covered by the structuring element B.

Morphological operators can be summarized into two fundamental operations: *erosion* $\varepsilon_B(g)$ and dilation $\delta_B(g)$ [2]. Basically, erosion deletes all pixels whose neighborhood cannot contain a certain structuring element (SE), i.e. it performs an intersection between the binary image g and B. On the contrary, dilation provides an expansion by addition of the pixels contained in the SE, i.e. a union between g and B.

Reconstruction filters provide an iterative reconstruction of the original image g starting from a mask I. If the mask I is the erosion $\varepsilon_B(g)$, the original brighter features are filtered by geodesic dilation (opening by reconstruction). On the contrary, if the mask I is the dilation $\delta_B(g)$, the original darker features are filtered by geodesic erosion (closing by reconstruction). A geodesic dilation (respectively erosion) is the pointwise minimum (maximum) between the dilation (erosion) of the marker image and the original image. Equation 15 and Equation 16 illustrate opening and closing by reconstruction, respectively:

$$\rho^{\uparrow}\delta\,[\varepsilon_{\downarrow}B\,(g)\,] = \rho^{\uparrow}\delta\,(I) = \min\{x^{\uparrow}g,\ \delta_{\downarrow}B^{\uparrow}k\,(I)\}\ |\ \delta_{\downarrow}B^{\uparrow}k\,(I) = \delta_{\downarrow}B^{\uparrow}(k-1)\,(I)$$

Equation 1

$$\rho^{\uparrow}\varepsilon\,[\delta_{\downarrow}B\,(g)\,] = \rho^{\uparrow}\delta\,(I) = \max\{x^{\uparrow}g,\ \varepsilon_{\downarrow}B^{\uparrow}k\,(I)\}\ |\ \varepsilon_{\downarrow}B^{\uparrow}k\,(I) = \varepsilon_{\downarrow}B^{\uparrow}(k-1)\,(I)$$

Equation 2

The reconstruction process is iterated until the reconstructed image at iteration k is identical to the image obtained at iteration $k-1$, i.e.:

$$\delta_B^k(I) = \delta_B^{k-1}(I)$$

Equation 3

$$\varepsilon_B^h(J) = \varepsilon_B^{h-1}(J)$$ **Equation 4**

in Equation 17 and Equation 18, respectively.

Using opening by reconstruction, the shape of the objects is preserved and the progressive increase of the size of the structuring element results in a progressive disappearance of objects whose pixels are eliminated by erosion using larger structuring elements. These objects cannot be recovered during the reconstruction. The size of the structuring element used in the reconstruction controls the strength of the reconstruction. Using larger structuring elements, peaks and valleys of the marker are filled (or taken out, respectively) quickly and only very bright (or dark, respectively) structures are recovered. On the contrary, using smaller size structuring elements in the reconstruction phase, the reconstruction is reached gradually and gray structures are also recovered.

CO-OCCURENCE TEXTURE MEASURES

Haralick et. al. (1972) [12] defined a set of texture measures for image processing derived from the so-called Gray Level Co-occurrence Matrix (GLCM). The GLCM measures the probability of occurrence of observing specific combinations of gray levels in the input image. Once the GLCM is computed, a set of statistics computed from the GLCM comprises the Haralick texture measures.

The Haralick Texture measures, or co-occurrence measures, are parameterized by the following:

- Texture Kernel Size – Defines a spatial area of interest for the texture computation. Typically square kernels are used but rectangular kernels are also possible.
- Quantization: Typically users of the co-occurrence metrics quantize the input data prior to computation of the GLCM matrix. Quantization is not strictly necessary and one may work with the same bit depth of the input data, however, the computation can be extremely slow and can consume a lot of memory. In this study the input data values were quantized to 16 input levels (i.e. 2^4).
- X, Y Offset – integer values of offset in the x and y directions. Vertical features can be assessed using an offset of 0 in the x direction and non-zero in the y direction; conversely horizontal features can be assessed using an non-zero offset in the x direction and a zero offset in the y direction. Non-zero offsets in both the x and y directions tend to probe features with arbitrary orientations. In principle one may compute a different GLCM for each s, y offset combination . In this study the x, y offsets were equal to ½ the texture kernel size.

Let $K_{i,j}$ represent the kernel matrix with elements i,j. A set of texture statistics can be computed using only the kernel matrix. This set is termed the "basic" texture descriptors. These are defined as follows:

Range: $$TRange = Max(K_{i,j}) - Min(K_{i,j})$$ **Equation 5**

Mean: $$TMean = \frac{1}{N}\sum_{i,j} K_{i,j}$$ **Equation 6**

Variance: $$TVar = \frac{1}{N-1}\sum_{i,j}(K_{i,j} - TMean)^2$$ **Equation 7**

Entropy: $$TEE = \sum_{i,j} K_{i,j}(-\ln K_{i,j})$$ **Equation 8**

Skewness: $$TSkew = \frac{1}{N}\sum_{i,j}\left(\frac{K_{i,j} - TMean}{\sqrt{Variance}}\right)^3$$ **Equation 9**

The co-occurrence texture statistics are computed from the GLCM matrix, which is derived from the kernel matrix. These statistics are defined as follows:

GLCM Contrast: $$TKContrast = \sum_{i,j} P_{i,j}(i-j)^2$$ **Equation 10**

GLCM Disimmilarity: $$TKDissim = \sum_{i,j} P_{i,j}|i-j|$$ **Equation 11**

GLCM Homogeneity: $$TKHomo = \sum_{i,j} \frac{P_{i,j}}{1+(i-j)^2}$$ **Equation 12**

GLCM Asymmetry: $$TKAsmm = \sqrt{\sum_{i,j} P_{i,j}^2}$$ **Equation 13**

GLCM Max Probability: $$TKMaxProb = Max(P_{i,j})$$ **Equation 14**

GLCM Entropy: $$TKEnt = \sum_{i,j} P_{i,j}(-\ln P_{i,j})$$ **Equation 15**

GLCM X Mean: $$TKMux = \sum_{i,j} iP_{i,j}$$ **Equation 16**

GLCM Variance: $$TKVar = \sum_{i,j} P_{i,j}(i-TKMux)^2$$ **Equation 17**

GLCM Correlation: $$TKCorr = \sum_{i,j} P_{i,j}\left[\frac{(i-TKMux)^2}{TKVar}\right]$$ **Equation 18**

where P_{ij} represents the GLCM matrix.

STUDY AREA

The study area includes the suburbs of Atlanta, Georgia USA. The same study area was used in [13]. The images were acquired by QuickBird on Feb 26 2007 (BEFORE) and by WorldView-1(AFTER) on October 21, 2007. The total study area comprises 25 square km's. The panchromatic band was used from Quickbird and compared to the panchromatic band on WorldView-1. For comparison purposes the images were registered prior to the change detection study and the WorldView-1 image was down-sampled to a spatial resolution of 0.6m.

Training data was digitized on the 25 square kilometer set. Two classes were identified, CHANGES and NO CHANGES. The CHANGES class comprised 67,087 pixels and represented primarily changes in large industrial or man-made structures. The NO CHANGES class comprised 68,497 pixels and consisted primarily of changes deemed uninteresting for this study, namely, changes in vegetation and land cover that weren't related to either new construction or residential development.

IMAGE PROCESSING

The images were processed through the following processing chain:

1. The AFTER image was radiometrically matched to the BEFORE image using a standard histogram matching process.
2. Both the BEFORE and AFTER images were processed with mathematical morphology operations consisting of an Opening of a Closing by reconstruction operation with a morphology kernel size of 15x15 for each operation. The resulting images are called $BEFORE_{MORPH}$ and $AFTER_{MORPH}$.

$$BEFORE_{MORPH} = Open(Close(BEFORE)) \quad \textbf{Equation 19}$$

$$AFTER_{MORPH} = Open(Close(AFTER)) \quad \textbf{Equation 20}$$

3. A difference image (DIFFERENCE) was created by taking the absolute difference of the $BEFORE_{MORPH}$ and $AFTER_{MORPH}$ images as follows:

$$DIFFERENCE = abs(AFTER_{MORPH} - BEFORE_{MORPH}) \quad \textbf{Equation 21}$$

4. Texture statistics were calculated from the DIFFERENCE image. Both basic texture statistics and co-occurrence texture statistics were generated for the following texture kernel sizes: 5x5, 15x15, 25x25, 51x51.

$$TEXTURE_{5x5} = Texture_{5x5}(DIFFERENCE) \quad \textbf{Equation 22}$$

$$TEXTURE_{15x15} = Texture_{15x15}(DIFFERENCE) \quad \textbf{Equation 23}$$

$$TEXTURE_{25x25} = Texture_{25x25}(DIFFERENCE) \quad \textbf{Equation 24}$$

$$TEXTURE_{51x51} = Texture_{51x51}(DIFFERENCE) \quad \textbf{Equation 25}$$

5. Each TEXTURE image was then combined with the training data to produce 4 statistics files suitable for ingest into the SpotFire Miner data mining package. Each statistics file is a comma separated value file format which contains all 14 texture attributes as columns, plus an extra column identifying the pixel as either changed (one) or not changed (zero). The number of rows in each file is equal to the total number of training samples (135,584).
6. Each statistics file was imported into SpotFire Miner[1] and a prediction model was built for each statistics file. The model workflow in SpotFire Miner included the following steps. For each statics file:
    a. The statistics file was imported into SpotFire Miner.
    b. The rows of the training data were shuffled in a random fashion to mix adjacent rows of CHANGE and NO CHANGE classes.
    c. The result was partitioned into two sets of data with 10% of the data acting as the training set and 90% of the data acting as the validation set.
    d. A Logistic Regression model [15] was trained on the training set.
    e. A prediction was performed using the validation set and the model formed in step (d).
    f. The prediction was validated against the known classes of the validation set. Classification statistics Precision, Recall and F-Measure were computed to assess the accuracy of the model in predicting the class of the validation set.

$$\text{Precision} = \frac{TP}{TP + FP} \quad \textbf{Equation 26}$$

$$\text{Recall} = \frac{TP}{TP + FN} \quad \textbf{Equation 27}$$

$$\text{FMeasure} = 2\frac{\text{Precision} * \text{Recall}}{\text{Precision} + \text{Recall}} \quad \textbf{Equation 28}$$

where TP is True Positive, FP is False Positive, and FN is False Negative.

7. As a final step a small 1000x1000 image chip was generated from each of the texture images. The chips were input into SpotFire Miner and classified using the Logistic Regression model trained for each dataset. The output of this process is a probability for each pixel that the pixel belongs to the CHANGE class.

[1] Spotfire Miner is a commercial data mining package available from Tibco Software.

RESULTS

The results on the imagery are shown in Figure 3. Referring to Figure 3, note that the processing of the BEFORE and AFTER images with the mathematical morphology operators tends to remove spatially tiny features from the imagery, like cars in the parking lot beside the large building in the lower right of (c) and (d), while preserving larger features in the imagery and preserving the sharp edges of the features. The degree of spatial filtering performed on the imagery can be controlled by selecting different kernel sizes for the morphology operation. In general using larger kernel sizes results in keeping larger features at the expense of removing smaller ones. The goal of this study was to detect changes in large urban features like land developments so a morphology kernel size of 15x15 was deemed appropriate.

The change detection images for each texture kernel are shown in (f), (g) and (h) in Figure 3, along with the absolute difference image derived from the difference between $AFTER_{MORPH}$ and $BEFORE_{MORPH}$, shown in (e). Note that the absolute difference image, even with significant spatial filtering using mathematical morphology, shows poor discrimination between CHANGE and NO CHANGE pixels. As the kernel size increases, the resulting change map becomes less and less sensitive to changes that are smaller than the size of the kernel. The change map shown in (h) was generated with a 51x51 kernel and shows changes only on those features which are on the scale of the kernel size or larger. The 51x51 kernel result suffers from some false positives due to shadows, visible in the upper right portion of the change map. Applying a shadow mask would improve the results.

The classification accuracy of each texture run was computed and appears in Table 1. The data is plotted in Figure 1. Note that both the precision values increase steadily with the increasing texture kernel size. The recall also increases steadily until the 51x51 kernel when it tends to dip down. This indicates that the false negative rate is slightly higher for the 51x51 kernel and indicates that some change is being missed. But balanced against the lower rate of false alarm the 51x51 kernel produces the best overall results according to the F-Measure statistic.

The logistic regression model outputs the ranking of the attributes using the Wald statistic [15]. This makes it possible to ascertain how important each of the feature attributes are to the overall discrimination of CHANGE versus NO CHANGE. The attribute ranking for all the attributes has been computed by summing up the values of the Wald statistic for each attribute and normalizing them to a common scale for comparison. The result appears in Figure 3.

Table 1. Classification accuracy results for the different texture kernel sizes.

Texture Kernel Size	Precision	Recall	F-Measure
5x5	0.9110	0.9622	0.9359
15x15	0.9388	0.9714	0.9548
25x25	0.9489	0.9774	0.9630
51x51	0.9656	0.9747	0.9701

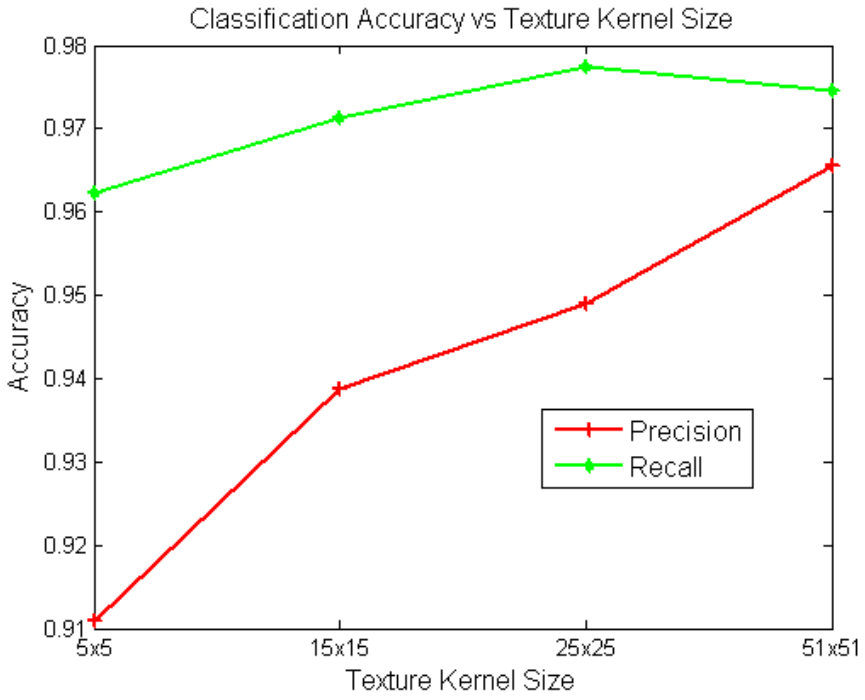

Figure 1. The classification accuracy as a function of the texture kernel size.

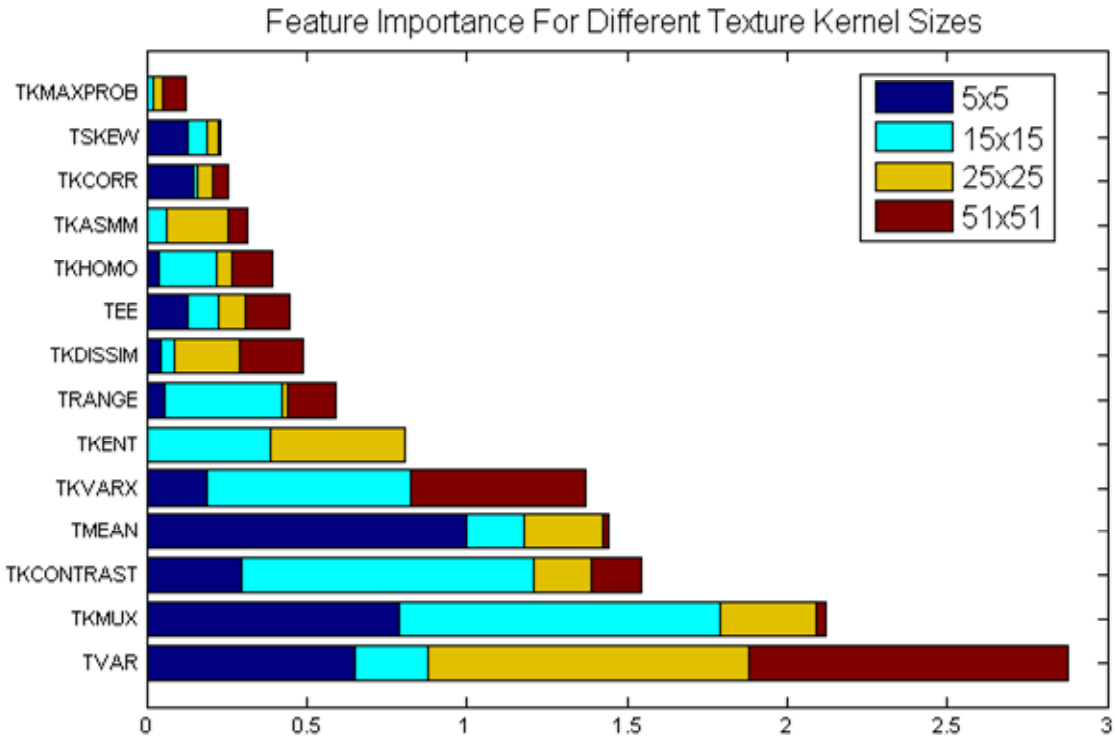

Figure 2. The feature attribute ranking for all the kernel sizes.

CONCLUSIONS

In this work we have applied mathematical morphology and co-occurrence texture statistics, along with data mining techniques to solve the change detection problem for a set of high spatial resolution images. Using a set of morphological operations on the before and after images, consisting of a closing of an opening by reconstruction operation, followed by processing the imagery with a 51x51 texture kernel and training a logistic regression model to classify the results, we have achieved a precision of 96.56% and a recall of 97.47%, for an overall classification accuracy of 97.01% (F-Measure) for the study area. We have observed a linear upward trend in the overall classification accuracy, determined by the F-Measure statistic, as the texture kernel size increases. We have ranked the importance of the texture attributes by their contribution to the overall classification solution using the Wald statistic. We have shown that some of the "basic" texture statistics are very useful for solving the classification problem, as the most important discriminating attribute was the variance of the pixels in the texture kernel itself (Figure 2). We have produced visual maps of the changes for different texture kernel sizes for a subset of the study area. The results show that as the texture kernel size increases, the change classification becomes less and less sensitive to changes in objects with smaller spatial scales.

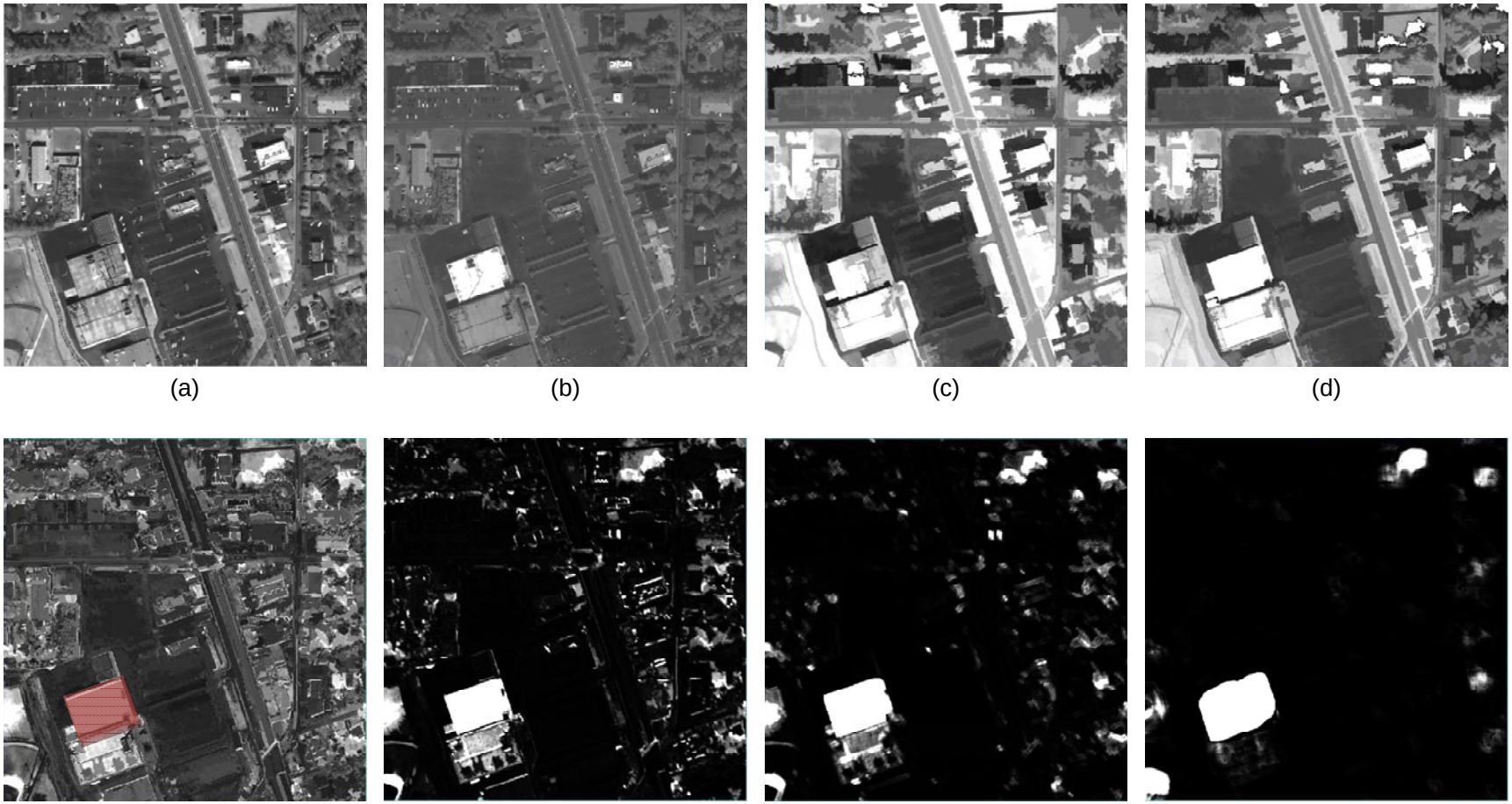

Figure 3. QuickBird panchromatic image BEFORE Feb 2007 (a), WorldView-1 Image AFTER Oct. 2007 (b), BEFORE image processed with morphological reconstruction (c), AFTER image processed with morphological reconstruction (d), the absolute difference (e) of (d) minus (c), the change map result for the 5x5 texture kernel (f), the change map result of the 15x15texture kernel (g), the change map result of the 51x51 texture kernel. The red pixels in (e) show the truth validation set for this image chip.

REFERENCES

1. S. R. Sternberg. Grayscale morphology, Computer Vision Graphics and Image Processing, vol 35, number 3, pages 333-355.
2. P. Soille, Morphological image analysis, Springer-Verlag, 2004, Berlin-Heidelberg.
3. M. Pesaresi and J. A. Benediktsson, A new approach for the morphological segmentation of high-resolution satellite images, IEEE transactions on Geosciences and Remote sensing, Feb 2001, vol. 39, number 2, pages 309-320.
4. P. Soille and M. Pesaresi, Advances in mathematical morphology applied to geoscience and remotesensing, IEEE Transactions on Geoscience and Remote Sensing, September 2002, vol 40, number 9, pages 2042-2055.
5. I. Epifanio and P. Soille, Morphological Texture Features for Unsupervised and Supervised Segmentations of Natural Landscapes, IEEE Transactions on Geoscience and Remote Sensing, April, 2007, vol. 45, number 4, pages 1074-1083.
6. M. Pesaresi and I. Kannellopoulos, Detection of urban features using morphological based segmentation and very high resolution remotely sensed data, Machine Vision and Advanced Image Processing in Remote Sensing, Springer Verlag, 1999, New York, NY.
7. J. A. Benediktsson and M. Pesaresi and K. Arnason, Classification and feature extraction for remote sensing images from Urban areas based on morphological transformations, IEEE Transactions on Geoscience and Remote Sensing, September, 2003, vol. 41, number 9, pages 1940-1949.
8. J. A. Benediktsson and J. A. Palmason and J. R. Sveinsson, Classification of hyperspectral data from urban areas based on extended morphological profiles, IEEE Transactions on Geoscience and Remote Sensing, march 2005, vol. 43, number 3, pages 480-490.
9. M. Fauvel and J. A. Benediktsson and J. Chanussot and J. R. Sveinsson, Spectral and Spatial Classification of Hyperspectral Data Using SVMs and Morphological Profiles, IEEE Transactions on Geoscience and Remote Sensing, November 2008, vol. 46, number 11, pages 3804-3814.
10. A. Plaza and P. Martinez and R. Perez and J. Plaza, A new method for target detection in hyperspectral imagery based on extended morphological profiles, Proceedings of IEEE Geoscience and Remote Sensing Symposium, 2003, vol. 6, pages 3772-3774, July, Toulouse, France.
11. A. Plaza and P. Martinez and J. Plaza and R. Perez, Dimensionality reduction and classification of hyperspectral image data using sequences of extended morphological transformations, IEEE Transactions on Geoscience and Remote Sensing, March 2005, vol. 43, number 3, pages 466-479.
12. Haralick et. al, Textural Features for Image Classification, , IEEE Transactions on Systems, Man, and Cybernetics, Vol @MC-3, No 6, November 1973.
13. F. Pacifici, C. Padwick, G. Marchisio, Unsupervised change detection frameworks for very high spatial resolution images, International Geoscience and Remote Sensing Symposium 2010, Honolulu, USA, July 25-30, 2010..
14. F. Pacifici, W. J .Emery, Pulse Coupled Neural Networks for Urban Change Detection at Very High Spatial Resolution, Iberomamerican Congress on Pattern Recognition, Guadalajara Mexico, Nov 15-18, 2009.
15. Hastie T, Tibshirani R, Friedman J. The elements of statistical learning: data mining, inference, and prediction. 2nd ed. Springer; 2009.